Sensors & Actuators: B. Chemical 369 (2022) 132372

Contents lists available at ScienceDirect

Sensors and Actuators: B. Chemical

journal homepage: www.elsevier.com/locate/snb

Compact breath monitoring based on helical intermediate-period fiber grating

Shen Liu [a,b,1], Wenqi Yan [a,b], Junlan Zhong [a,b], Tao Zou [a,b], Min Zhou [a,b], Peijing Chen [a,b], Hang Xiao [a,b], Bonan Liu [a,b], Zhiyong Bai [a,b,*,2], Yiping Wang [a,b]

[a] Shenzhen Key Laboratory of Photonic Devices and Sensing Systems for Internet of Things, College of Physics and Optoelectronic Engineering, Shenzhen University, Shenzhen 518060, China

[b] Guangdong and Hong Kong Joint Research Centre for Optical Fiber Sensors, Shenzhen University, Shenzhen 518060, China

ARTICLE INFO

Keywords:
Helical intermediate-period fiber grating
Breath sensor
Optical fiber sensor
Humidity sensor

ABSTRACT

Tiny and soft breath sensors offer unique capabilities in a continuous and long-term recording of vital physiological parameters for human health monitoring. Here, we propose an all fiber-optic breath sensor based on helical intermediate-period fiber grating (E-HIPFG) written in an elliptic core polarization-maintaining fiber. This E-HIPFG-based breath sensor shows ultrafast response time and recovery time, which are 34.46 ms and 41.34 ms, respectively. The response time and recovery time are three orders faster than the corresponding values of conventional optical fiber-based breath sensors with humidity-sensitive material. In addition, this sensor does not combine with any additional coating materials or fiber architectures, increasing the stability in a continuous and long-term detection for breath monitoring. The E-HIPFG sensor is insensitive to external influences, such as temperature, torsion and strain, endowing the possibility of stable detection in the moving body. Particularly, the temperature sensitivity of the sensor is 2.75 pm/°C, which is two orders lower than the corresponding value of previous reports. Due to its considerable stability, quick response, and insensitivity to external influences, the E-HIPFG-based breath sensor offers significant potential for long-term and compact breathing monitoring devices.

1. Introduction

Stable long-term monitoring of breath can provide practical diagnostic information for patients with breath disorders, heart failure or health rehabilitation training [1–3]. Spirometry, pneumotacography, and optoelectronic plethysmography are the frequently used techniques at present, which are normally complicated, high cost and bulky [1,2,4]. In addition, mouthpieces, masks, and other equipment needed by the medical system may interfere with natural breathing and limit human activities. In addition, external equipment, such as mouthpieces and masks are required by the medical system, conventional pressure-based breath sensors frequently suffer from the sensor strain and deformation brought by human body movement [5,6], making them unsuitable for a long-term wearable device.

Based on the previous research reported by Maiti et al., water molecules account for a larger proportion in the breath air than other trace chemicals [7]. Therefore, alternative strategies for breath monitors based on the humidity difference between indoor humidity (30-60% RH) and human exhalation (around 70–90%RH) under the nose have been intensively investigated [8]. The research and development of humidity sensing have a long history [9–11], and there is a variety of sensing technologies that have achieved industrial-related humidity measurements, such as mechanical hygrometers, chilled mirror hygrometers, and wet and dry bulbs psychrometers. However, these traditional methods are either unstable in environmental conditions or susceptibility to surface contaminations, or unwearable [12]. In this case, the optical humidity sensor has the characteristics of anti-electromagnetic interference, high repeatability, small size, strong adaptability, and quick response [13–22].

Over the past three decades, numerous optical fiber-based humidity

* Corresponding author at: Shenzhen Key Laboratory of Photonic Devices and Sensing Systems for Internet of Things, College of Physics and Optoelectronic Engineering, Shenzhen University, Shenzhen 518060, China.

E-mail addresses: shenliu@szu.edu.cn (S. Liu), baizhiyong@szu.edu.cn (Z. Bai).

[1] orcid.org/0000-0001-9266-2498

[2] orcid.org/0000-0002-0915-751X

https://doi.org/10.1016/j.snb.2022.132372
Received 20 April 2022; Received in revised form 21 June 2022; Accepted 12 July 2022
Available online 19 July 2022

sensors for breath monitoring have been proposed and developed tremendously. Arregui et al. proposed an optical fiber humidity sensor based on Fabry-Perot structure coated with ionic self-assembly polymeric material. Their result demonstrated a response time of 1.5 s in humidity monitoring [13]. In 2018, Dissanayake et al. prepared long-period gratings (LPFG) with a grating length of 25 mm, which showed 0.15 dB/% RH and 0.32 nm/°C for humidity and temperature after coating the surface with GO [19]. Du et al. investigated a length of 15 mm etched single-mode fiber (SMF) coated with MoS_2 to detect breath, achieving a response of 0.066 s and a recovery time of 2.395 s [22]. More recently, in 2020, the team also tested the relative humidity of 11–92%RH using gold nanomembrane onto the end-face of optical fiber and found that the response time and recovery time were 156 ms and 277 ms, respectively [21]. Nevertheless, most of those optical fiber-based humidity sensors are based on the adsorption and desorption of water molecules by the moisture-sensitive materials on the transducer surface, which prolongs the sensing response time. In clinical practice, the breath cycle is about 3–5 s, which means a higher requirement for breath response or recovery time in such a short period so as to restore the signal with as little loss of authenticity as possible. In addition, the utilization of moisture-sensitive materials leads to a more complex sensor structure and reduces the sensor's mechanical strength and compactness, subsequently decreasing the sensor stability for long-term monitoring and limiting their practical application.

This work introduces a compact, high stability, and ultrafast-response fiber-optic breath sensor based on an elliptic core helical intermediate-period fiber grating (E-HIPFG). The topographic characteristics and optical features of the E-HIPFG-based breath sensor, which is fabricated by hydrogen-oxygen flame heating, are analyzed at first. The stability of the HIPFG is demonstrated with considerably low sensitivity to environmental disturbances, including temperature, strain, and torsion. The response time and recovery time are further studied to access the sensing performances for real human breath monitoring. The results demonstrate that the E-HIPFG-based breath sensor has considerable stability, ultrafast-response, and insensitivity to environmental factors, and is promising for long-term and compact breathing monitoring devices.

2. E-HIPFG fabrication

The E-HIPFG was fabricated on an elliptical core polarization-maintaining fiber (PMF) (Yangtze Optical Electronic Co., Ltd.) with two-fold symmetry in the cross-section, as shown in Fig. 1(a). The elliptical core diameters along the major and minor axes of the PMF are 9.6 and 5.0 μm, respectively. The E-HIPFG was fabricated by a hydrogen-oxygen flame heating system, consisting of a high-precision rotator, two translation stages, and a hydrogen generator (Model TH-500, China). The fabrication process was detailed described in our previous reports [23,24]. Briefly, the PMF is fixed on two translation stages. When the translation stages were working with velocities of $V_1 = 1.10$ mm/s and $V_2 = 1.20$ mm/s, and the rotation motor was rotating at a speed of 2057 rpm, the hydrogen-oxygen flame produced by the hydrogen generator was employed to heat the fiber to its melting point.

After the grating was inscribed on the fiber, the size of the major and minor axes of the fiber core was reduced to 8.7 μm and 4.9 μm, respectively. And the cladding diameter was reduced from 120 to 110 μm, as shown in Fig. 1(b). Then both ends of the 2.02 mm-grating length E-HIPFG were spliced with SMF, as shown in Fig. 1(c). The E-HIPFG has a helical pitch of 17.5 μm, as illustrated in scanning electron microscope images Fig. 1(d). The torsion deformation caused by stress was manifested in the periodic physical deformation on the fiber surface and periodic perturbations in the fiber core. Because the gratings in the intermediate period were written on the elliptical core PMF with the intrinsic major and minor axes structure of the fiber core, the bi-taper of E-HIPFG within a helical period is more obvious than the SMF under a microscope observation [25,26].

The E-HIPFG was launched by an amplified spontaneous emission source (ASE, NKT Photonics) and its transmission spectra were recorded by an optical spectrum analyzer (OSA, YOKOGAWA, AQ6370C) with a resolution of 0.05 nm. The transmission spectrum of the E-HIPFG in the air is shown in Fig. 2. In a wavelength range of 1300–1650 nm, four resonant dips appear at 1351.7 nm (Dip-1), 1432.01 nm (Dip-2), 1519.13 nm (Dip-3), and 1611.16 nm (Dip-4) and the maximum attenuation is 31.335 dB at the Dip-4. These resonant dips result from the optical coupling between the fundamental core mode and cladding

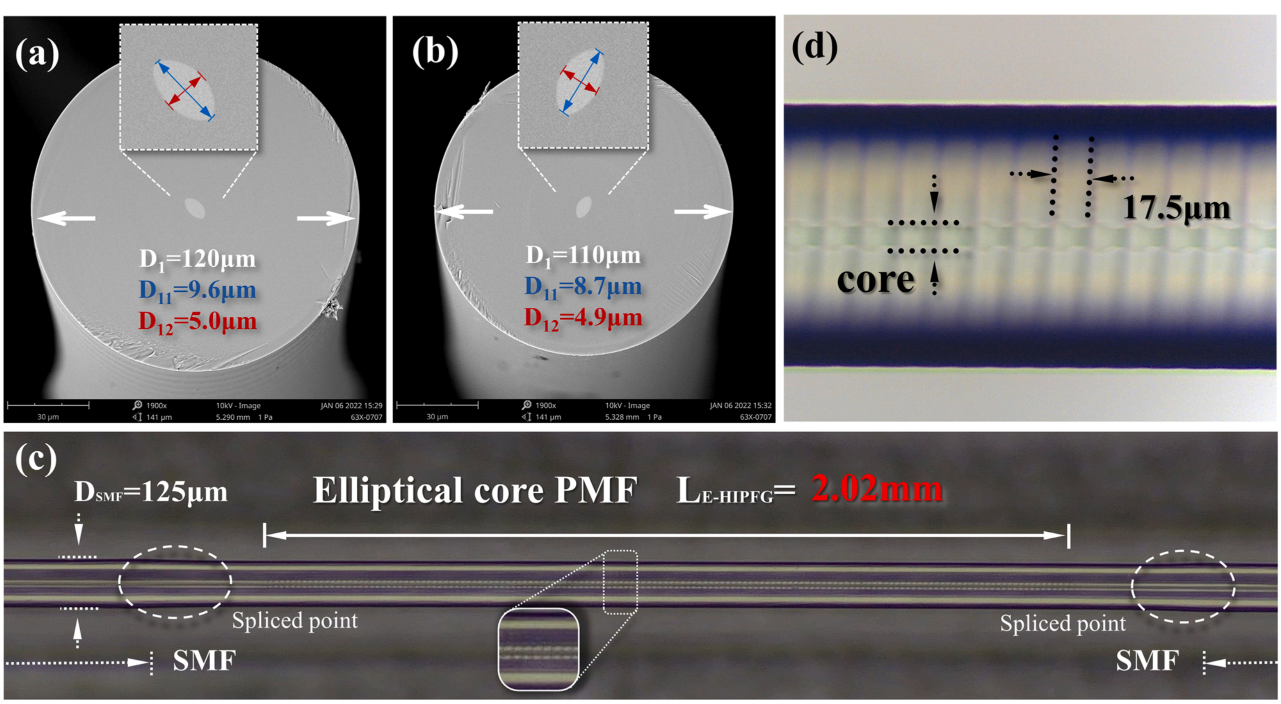

Fig. 1. The topographic characteristics of the E-HIPFG. Scanning electron micrographs of the cross-section of the elliptical core PMF (a) before and (b) after E-HIPFG inscribed in, (c) the total view of the E-HIPFG observed by microscope, inset figure is the enlarged view of the fiber core, (d) the side-view of the E-HIPFG.

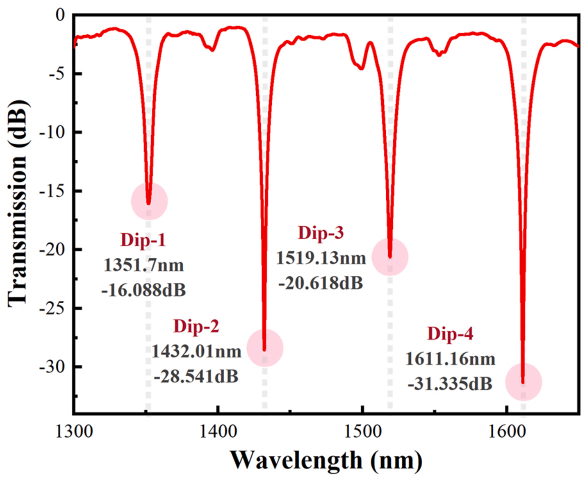

Fig. 2. The transmission spectrum of E-HIPFG in air.

mode in the fiber in the phase-matching condition, and the resonance wavelengths of these dips can be expressed as [27].

$$\lambda_{res} = \left(n_{co}^{eff} - n_{cl,m}^{eff}\right)\Lambda$$

where, λ_{res} is the phase-matched resonance wavelength corresponds to the mth cladding mode; n_{co}^{eff} and $n_{cl,m}^{eff}$ corresponds to the effective refractive index of the fundamental core mode and the mth cladding mode respectively; Λ is the grating period, which can be achieved by the formula of $\Lambda = 30\ V_2/\Omega$, where is the velocities of translation stages and Ω is the speed of rotating. By comparing the grating period of HIPFG in SMF prepared under the same fabrication parameters, E-HIPFG has a half grating period due to the unique double symmetric structure of the elliptic core of the PMF. Therefore, the number of periods of E-HIPFG is twice more than that of HIPFG in the case of the same grating length, which reduces the grating length and optimizes the integration characteristics for portable breath monitors.

3. Sensing properties of the E-HIPFG-based breath sensor

3.1. RI sensitivity

Since breath monitoring of the E-HIPFG is based on a change of the effective RI induced by breath, describing the E-HIPFG's RI sensitivity is required. The RI matching liquids (Cargille Labs) with an RI from 1.300 to 1.370 were utilized to obtain the RI sensitivity. In the measurement, the whole E-HIPFG sample was immersed in the RI matching solution and the transmission spectra covering from 1300 nm to 1650 nm were recorded. After each measurement, a careful clean-and-dry process was conducted to remove residual liquid on the surface of the device until the transmission spectrum returns to its original.

Fig. 3(a) illustrates the resulted spectra around Dip-4 in various RI matching liquids, where a redshift happens to the resonance wavelength. The function of resonant wavelength versus surrounding RI is shown in Fig. 3(b). Similar to the research of Zou [28], the resonant wavelength drift increases nonlinearly with the increase of the surrounding RI.

Among those dips, the average refractive index sensitivities of the four resonant wavelengths are 176.43 nm/RIU at Dip-1, 233.0 nm/RIU at Dip-2, 331.7 nm/RIU at Dip-3 and 380.29 nm/RIU at Dip-4, respectively. Within the same refractive index range, it can be seen that when the surrounding refractive index is smaller than the cladding refractive index, the resonant wavelength of long wave length changes more for the external refractive index, and its perception ability of minor alterations is better than the resonant wavelength of shorter wavelength, which is consistent with the analytical formula [29].

$$\frac{d\lambda_{res}}{dn_{sur}} = \lambda_{res} \cdot \gamma \cdot \Gamma_{sur}$$

Therefore, the Dip-4 with maximum sensitivity 380.29 nm/RIU is chosen to evaluate the detection performance of the E-HIPFG sensor. Compared with the HIPFG reported by Zou in 2021 [28], In 2020, Luo et al. used arc discharge (EAD) technology to fabricate long-period fiber gratings in thin-clad fibers to obtain sensing characteristics with RIS of − 51.72 nm/RIU [30]. Wang et al. proposed a core-shift microstructure interferometer sensor with its RIS of 56.325 nm/RIU [31]. The average RIS of E-HIPFG suggested in this study is approximately 7 times that of the research results of Luo and Wang. On the other hand, the RIS with interferometers normally have much higher RIS than the E-HIPFG. However, those interferometers often suffer from high temperature-cross-sensitivity. Luo et al., fabricated a Mach–Zehnder interferometer (MZI) on multi-mode fiber with the RIS of 2576.584 nm/RIU and the temperature sensitivity of 0.193 nm/°C [32]. Another MZI in single-mode fiber developed by Liao et al. has a RIS of 4202 nm/RIU and the temperature sensitivity of 41 pm/°C [33]. The E-HIPFG in this work gives a low temperature sensitivity of 2.79 pm/°C, which is two orders lower than Luo's research results and one-fifteenth of that of Liao's. The details will be explained in Section 3.3.

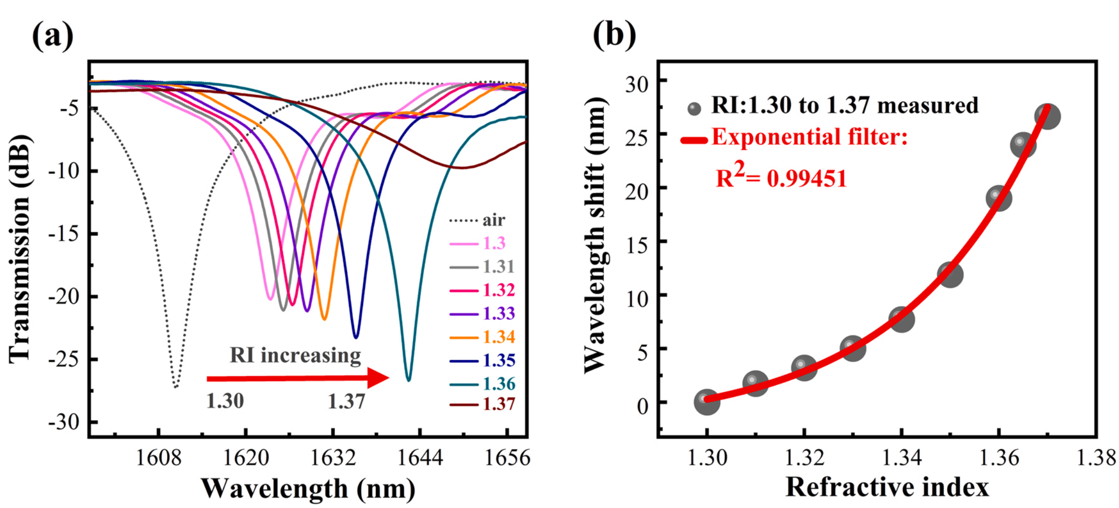

Fig. 3. (a) Dip-4 spectra at RI range from 1.300 to 1.370; (b) Relationship between resonant wavelength and the surrounding RI.

3.2. Breath monitoring

The humidity experiment was carried out in a sealed box at room temperature. An optical power meter (Keysight, N7744A) with a resolution of 0.3 pm and a tunable laser (Keysight, 81940A) were used to test and record the relationship between humidity and spectrum drift of E-HIPFG at 10–99% RH, as shown in Fig. 4(a). Fig. 4(b) illustrates the transmission spectra of the E-HIPFG around Dip-4 in the humidity range of 60–99%RH. The resonant wavelength gradually redshifts with the increase of humidity, and the peak of coupling wavelength and humidity shows a non-linear relationship which is similar to Bao's research in 2021 [34]. Notably, the wavelength shift at humidity below 60%RH is nearly a constant because the RI change caused by low water vapor concentration is unnoticeable. When the humidity is over 60%RH, which is the humidity range close to normal human breath [8], the wavelength shift increases significantly. In the humidity range of 60–99%RH, the wavelength shift and the humidity present an index function with the maximum sensitivity of 4.78 pm/%RH at 99%RH.

To further assess the sensing performance of the E-HIPFG sensor, the reaction time and recovery time, which are essential parameters for real human breath monitoring, are investigated by a system with a tunable laser (Agilent 81940A), photodetector (PD, Newport Model 1544-B) and oscilloscope (Tektronix, MDO3054) as shown in Fig. 5(a). In the test, the E-HIPFG was inserted in bi-nasal intubation shown in Fig. 5(b) and fixed to the volunteer's nose, as shown in the inset figure of Fig. 5(a). Fig. 5(c) shows the E-HIPFG illuminated with white light, demonstrating the sensor's device size through colored diffraction light. The wavelength of the tunable laser was fixed at 1611.16 nm, which is the resonance wavelength of Dip-4 in an air medium. The wavelength shift of Dip-4 was monitored with inhaled and exhaled human breath at room temperature.

The breath status of volunteers during rest (normal breathing), strenuous exercise (rapid breathing), and complete relaxation (slow breathing) were monitored for 20 s by the E-HIPFG and the response features are shown in Fig. 6(a)-(c). The time responses in a single breath were shown in Fig. 6(d)-(f). The breathing frequencies were obtained by Fast Fourier transforms (FFT) (see Fig. 6(g)–(i)).

At rest state, the response time and the recovery time of normal breathing are determined to be approximately 54.56 ms and 64.70 ms as shown in Fig. 6(d). Through FFT, the breathing frequency of volunteers can be clearly and succinctly identified. It can be seen that the normal breathing rate is 0.25 Hz, which is consistent with the range of human breathing frequency (12–20 breaths per minute). In a strenuous exercise state, the breath period is much shorter than normal breath, as presented in Fig. 6(b). In this state, the response time and the recovery time are 34.46 ms and 41.34 ms, respectively. And the breathing rate is 1.05 Hz. When the volunteer is completely relaxing, the response time, the recovery time, and breath frequency are 253.56 ms, 346.72 ms and 0.15 Hz. The response time and recovery time of the breath sensor are shortened with the increase of breath frequency with the fastest response time and recovery time being 34.46 ms and 41.34 ms. This may be because in a faster breath state, the humidity near the volunteer's increases faster than the slower one's. In summary, the varied breath states are represented by the different response durations and breath frequencies, suggesting that the proposed sensor can achieve high resolution and accuracy for real-time breath monitoring.

3.3. Anti-interference capacity test

Since the phase-matching condition shows that the resonant wavelength is primarily determined by the effective refractive index of the coupling mode and the grating period, any change in the strain, temperature, twist caused by body movement may result in a large shift in the resonance wavelength shift. Therefore, the effect of those factors on the E-HIPFG should be evaluated before sensing application. Firstly, the temperature response of the prepared E-HIPFG was investigated by putting it into a column oven (LCO 102, ECOM) with a temperature range from 25° to 95°C. The transmission spectra of the E-HIPFG were recorded when the temperature was stabilized for 10 min with the step of 10 °C, as shown in Fig. 7(a). The resonant dip of the E-HIPFG redshifts and the coupling strength becomes deeper when the temperature increases from 25 °C to 95 °C. Fig. 7(b) presents the function of resonance wavelength shift with the temperature increase. The temperature sensitivity of E-HIPFG is calculated to be 2.79 pm/°C according to the slope of the fitting line. In a realistic application, the greatest temperature difference between inhaled and exhaled air is less than 3 °C [35], hence the wavelength shift induced by temperature difference is less than 8.4 pm, which is about 10% of the wavelength shift generated by humidity (approximately 86 pm). The variation in temperature has no significant effect on the frequency characteristics of breath with such a measurement error.

On the other hand, in the process of sensor packaging before application, there will be strain and torsion differences before and after the procedure. In addition, differences in the packaging process result in different strains and torsions that will affect the uniformity of the sensor. Therefore, insensitivity to strain and torsion characteristics are essential for the sensor's stability and uniformity. In the torsion test, a rotating fixture was applied to rotate E-HIPFG to + 360° at first. Then the E-

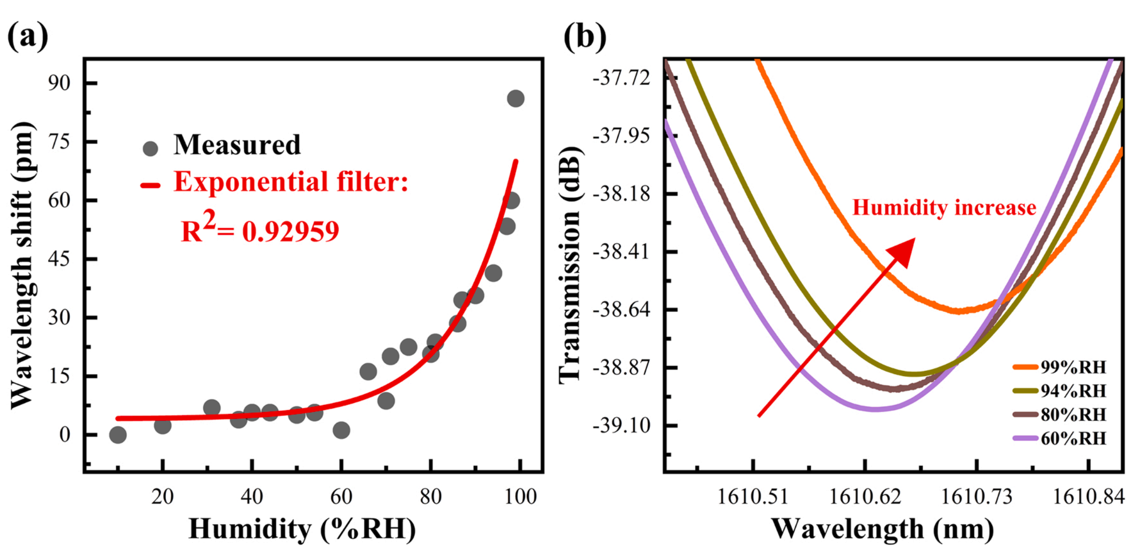

Fig. 4. (a) The relationship between wavelength shift and humidity; (b) The transmission spectra of the E-HIPFG around Dip-4 in the humidity range of 60–99%RH.

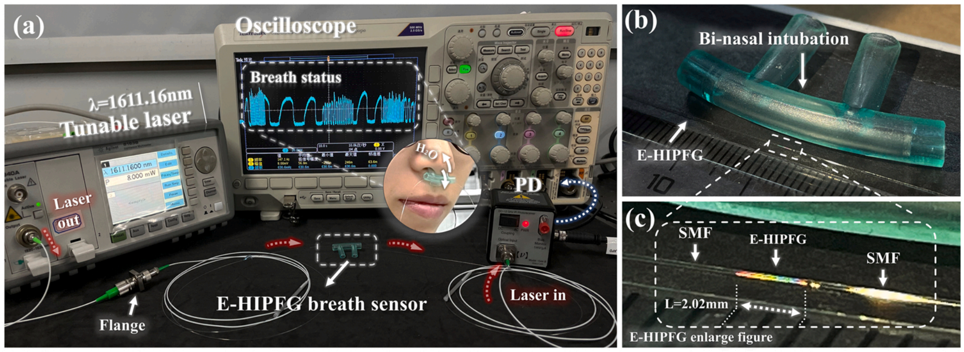

Fig. 5. (a) The breath experiment setup; (b) Detail view of the Bi-nasal intubation and unapplied E-HIPFG; (c) Partial enlargement of E-HIPFG.

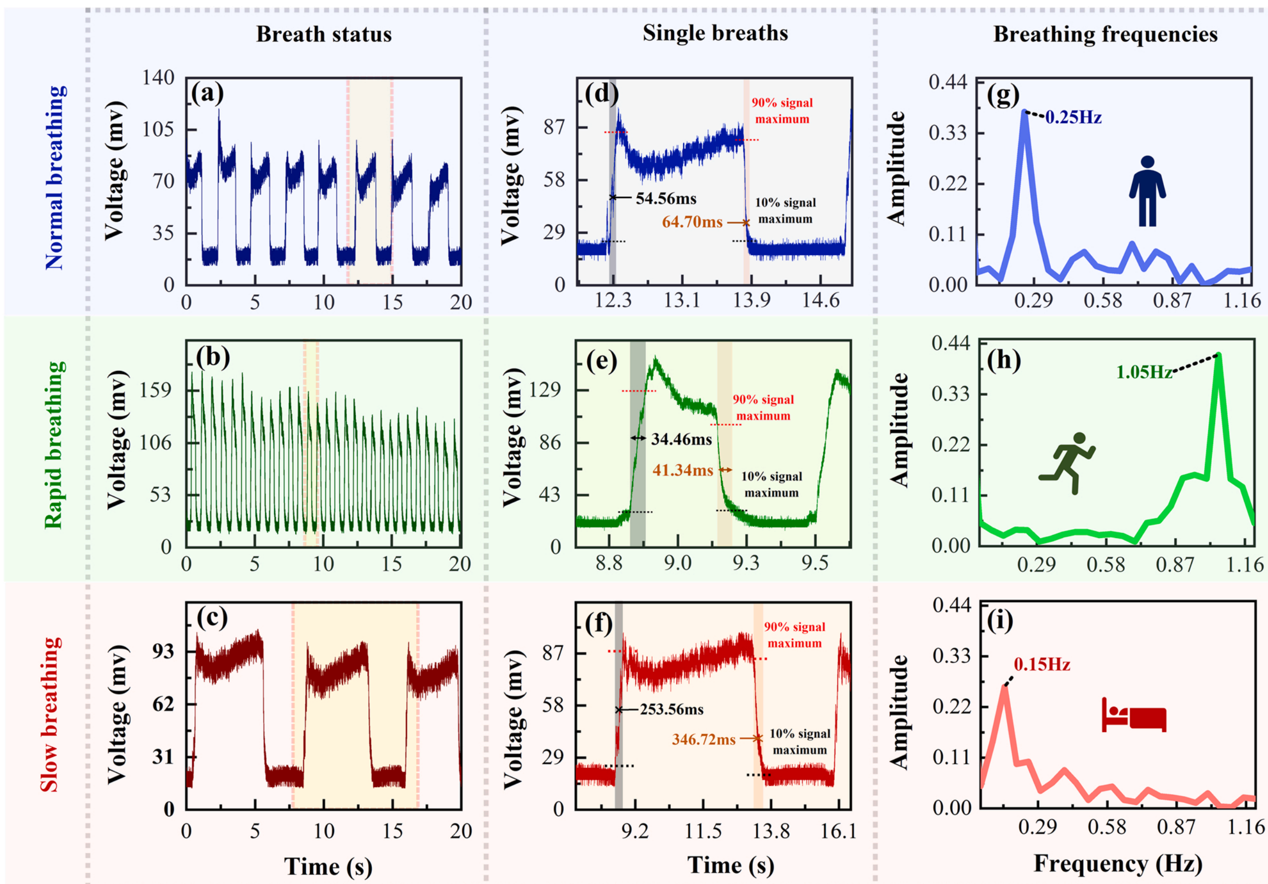

Fig. 6. The real-time response of the E-HIPFG-based breath sensor to normal breathing (a), rapid breathing (b), and complete slow breathing (c) were monitored, and their time responses in a single breath (d-f), and their breathing frequencies (g-i).

HIPFG was twisted from + 360° to − 360° with a step of 30°. The torsion rate is defined as $\gamma = \theta/L$, which means to represent the torsional stress applied per unit length, where θ is the rotation angle, and L is the distance between two fixed points, which is 20 cm. The rotation has the same direction (+360°−0°) with the HIPFG sample torsion is defined as clockwise rotation and counterclockwise versa (−360°−0°). The resulted spectra and the function between wavelength shift and torsion are represented in Fig. 7(c) and (d), with the torsion sensitivity determined to be − 23.937 nm/(rad/mm). Similar to the torsion experiment, the transmission spectra of E-HIPFG were collected with the strain range 0–2000 με by adjusting the coaxial moving distance with a high-precision displacement platform. As shown in Fig. 7(e) and (f), with the application of transverse strain, the wavelength of E- HIPFG blue-shifts and the coupling depth deepens, and the strain sensitivity is 0.588 pm/με by fitting the dip of wavelength change with the corresponding slope.

3.4. Sensing properties comparison

The sensing properties of the humidity sensor based on LPFG are compared in this part, with the details listed in Table 1. As we mentioned in Section 1, most of the humidity sensors are combined with moisture-sensitive materials, which prolong the response times and recovery times. The E-HIPFG-based breath sensor described in this paper has outstanding response and recovery times, which are nearly three orders faster than the valued of the previous breath sensor explored by Xu in 2021 [36]. The response time and recovery time of the E-HIPFG-based sensor are also improved when compared to conventional optical

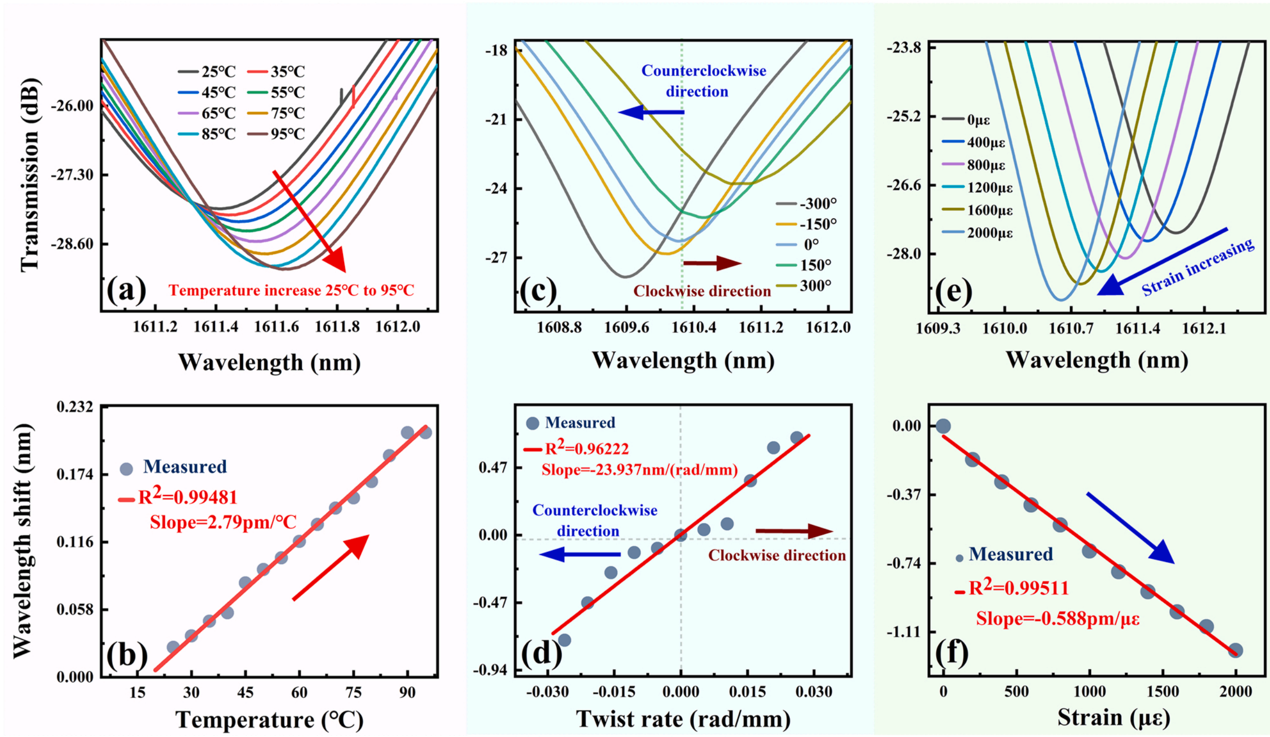

Fig. 7. The stability analysis of the E-HIPFG. Spectra and wavelength shift relationship of Dip-4 in varying temperature (a-b), torsion (c-d), strain (e-f).

Table 1
Comparison of the performance of humidity sensor based on LPFG for grating length, period, temperature sensitivities, response time and recovery time.

Humidity sensor	Sensitized material type	Grating period (μm)	Length (mm)	Response time (s)	Recovery time (s)	Temperature (pm/°C)	Ref
LPFG on SMF	Polyethylene glycol (PEG) and polyvinyl alcohol (PVA)	300	180	0.63	/	-430	[37]
LPFG on SMF	Silica nanoparticles	110.9	40	/	/	250	[39]
LPFG on SMF	SiO_2 nanospheres	395	41	0.1–0.2	/	/	[41]
LPFG on SMF	Silica nanoparticles	108	30	/	/	-147	[38]
LPFG in solid-core PCF	Graphene oxide (GO)/cellulose acetate (CA) composites	410	2.8	32	68	/	[36]
LPFG on multi-mode cyclic transparent optical polymer fiber	None	155	2	7500	5400	-102	[40]
E-HIPFG on PMF	None	**17.5**	**2.02**	**0.035**	**0.041**	**2.79**	**This work**

fiber-based sensors, as shown in Table 1. The fast response time and recovery time can be attributed to the fact that the E-HIPFG sensor does not use any sensitive material, reducing the time to absorb and desorb water molecules. Furthermore, the inaccuracy generated by the interaction of sensitive material with water molecules can be avoided, resulting in increased sensing accuracy. In particular, in 2019, Theodosiou introduced a humidity sensor based on LPFG that did not require coating sensitive material but had a relatively lengthy response and recovery time. Furthermore, the E-HIPFG-based sensor also shows fairly low temperature, torsion, and strain sensitivity. Notably, the sensor's temperature sensitivity is 2.75 pm/°C, which is two orders lower than prior reports' values [37–40]. The E-HIPFG can be a contender for building novel high stability sensors due to its quick reaction time and recovery time as well as low temperature, torsion, and strain sensitivity, allowing it to be integrated into breathing equipment such as breathing tubes, oxygen masks, and nasal straws.

4. Conclusion

The E-HIPFG-based breath sensor, without external materials or restructuring, is proposed and demonstrated with considerable stability and ultra-fast response time and recovery time. The sensor presents a superior response time of 34.46 ms and a recovery time of 41.34 ms, which are much faster than these values of the conventional optical fiber-based methodologies. The stability of the sensor is demonstrated by its insensitivity to low sensitivity to temperature, torsion, and strain, which makes it stable for wearable and mobile sensing in compact devices. Furthermore, this sensor does not require any extra coating materials or fiber designs, resulting in increased stability in continuous and long-term breath monitoring detection. Therefore, E-HIPFG shows a better performance for real-time breath monitoring, attributed to its less chemical modification and intrinsic chemical stability. Hence the proposed breath monitor can be considered to have a broad application prospect in breath monitoring and portable medical devices due to its exceptional sensing properties.

CRediT authorship contribution statement

Shen Liu: Conceptualization, Methodology, Writing-Original draft preparation, Funding acquisition, **Wenqi Yan** Conceptualization, Methodology, Writing-Original draft preparation, **Junlan Zhong**: Conceptualization, Methodology, **Tao Zou**: Investigation, **Min Zhou**:

Visualization, **Peijing Chen**: Writing-Reviewing and Editing. **Hang Xiao**: Resources, **Bonan Liu**: Resources, **Zhiyong Bai**: Funding acquisition. **Yiping Wang**: Project administration, Supervision.

Declaration of Competing Interest

The authors declare that they have no known competing financial interests or personal relationships that could have appeared to influence the work reported in this paper.

Acknowledgments

This study was supported by the National Natural Science Foundation of China (NSFC) (62175165 and 61905165); Guangdong Basic and Applied Basic Research Foundation (2021A1515011834, 2019A050510047); and Shenzhen Science and Technology Program (grant nos. RCBS20200714114922296 and JCYJ20210324120403009).

References

[1] C. Massaroni, D. Lo Presti, D. Formica, S. Silvestri, E. Schena, Non-contact monitoring of breathing pattern and respiratory rate via RGB signal measurement, Sensors 19 (2019), https://doi.org/10.3390/s19122758.
[2] H. Liu, J. Allen, D. Zheng, F. Chen, Recent development of respiratory rate measurement technologies, Physiol. Meas. 40 (2019) 07TR1, https://doi.org/10.1088/1361-6579/ab299e.
[3] M. Beaumont, P. Forget, F. Couturaud, G. Reychler, Effects of inspiratory muscle training in COPD patients: a systematic review and meta-analysis, Clin. Respir. J. 12 (2018) 2178–2188, https://doi.org/10.1111/crj.12905.
[4] A. Aliverti, R. Dellaca, P. Pelosi, D. Chiumello, L. Gatihnoni, A. Pedoti, Compartmental analysis of breathing in the supine and prone positions by optoelectronic plethysmography, Ann. Biomed. Eng. 29 (2001) 60–70, https://doi.org/10.1114/1.1332084.
[5] M. Li, H. Li, W. Zhong, Q. Zhao, D. Wang, Stretchable conductive polypyrrole/polyurethane (PPy/PU) strain sensor with netlike microcracks for human breath detection, ACS Appl. Mater. Interfaces 6 (2014) 1313–1319, https://doi.org/10.1021/am4053305.
[6] L.Q. Tao, K.N. Zhang, H. Tian, Y. Liu, D.Y. Wang, Y.Q. Chen, et al., Graphene-paper pressure sensor for detecting human motions, ACS Nano 11 (2017) 8790–8795, https://doi.org/10.1021/acsnano.7b02826.
[7] K.S. Maiti, M. Lewton, E. Fill, A. Apolonski, Sensitive spectroscopic breath analysis by water condensation, J. Breath. Res 12 (2018), 046003, https://doi.org/10.1088/1752-7163/aad207.
[8] S. Kano, K. Kim, M. Fujii, Fast-response and flexible nanocrystal-based humidity sensor for monitoring human respiration and water evaporation on skin, ACS Sens. 2 (2017) 828–833, https://doi.org/10.1021/acssensors.7b00199.
[9] H. Hammouche, H. Achour, S. Makhlouf, A. Chaouchi, M. Laghrouche, A comparative study of capacitive humidity sensor based on keratin film, keratin/graphene oxide, and keratin/carbon fibers, Sens. Actuators A Phys. 329 (2021), https://doi.org/10.1016/j.sna.2021.112805.
[10] M.A. Najeeb, Z. Ahmad, R.A. Shakoor, Organic thin-film capacitive and resistive humidity sensors: a focus review, Adv. Mater. Interfaces 5 (2018), https://doi.org/10.1002/admi.201800969.
[11] A. Rianjanu, T. Julian, S.N. Hidayat, N. Yulianto, N. Majid, I. Syamsu, et al., Quartz crystal microbalance humidity sensors integrated with hydrophilic polyethyleneimine-grafted polyacrylonitrile nanofibers, Sens. Actuators B Chem. 319 (2020), https://doi.org/10.1016/j.snb.2020.128286.
[12] T.L. Yeo, T. Sun, K.T.V. Grattan, Fibre-optic sensor technologies for humidity and moisture measurement, Sens. Actuators A Phys. 144 (2008) 280–295, https://doi.org/10.1016/j.sna.2008.01.017.
[13] F.J. Arregui, Y. Liu, I.R. Matias, R.O. Claus, Optical fiber humidity sensor using a nano Fabry–Perot cavity formed by the ionic self-assembly method, Sens. Actuators B Chem. 59 (1999) 54–59, https://doi.org/10.1016/s0925-4005(99)00232-4.
[14] A. Gaston, F. Perez, J. Sevilla, Optical fiber relative-humidity sensor with polyvinyl alcohol film, Appl. Opt. 43 (2004) 4127–4132, https://doi.org/10.1364/ao.43.004127.
[15] M. Yinping, L. Bo, Z. Hao, L. Yuan, Z. Haibin, S. Hua, et al., Relative humidity sensor based on tilted fiber bragg grating with polyvinyl alcohol coating, IEEE Photonics Technol. Lett. 21 (2009) 441–443, https://doi.org/10.1109/lpt.2009.2013185.
[16] L. Alwis, T. Sun, K.T.V. Grattan, Fibre optic long period grating-based humidity sensor probe using a Michelson interferometric arrangement, Sens. Actuators B Chem. 178 (2013) 694–699, https://doi.org/10.1016/j.snb.2012.11.062.
[17] D. Su, X. Qiao, Q. Rong, H. Sun, J. Zhang, Z. Bai, et al., A fiber Fabry–Perot interferometer based on a PVA coating for humidity measurement, Opt. Commun. 311 (2013) 107–110, https://doi.org/10.1016/j.optcom.2013.08.016.
[18] A. Urrutia, J. Goicoechea, A.L. Ricchiuti, D. Barrera, S. Sales, F.J. Arregui, Simultaneous measurement of humidity and temperature based on a partially coated optical fiber long period grating, Sens. Actuators B Chem. 227 (2016) 135–141, https://doi.org/10.1016/j.snb.2015.12.031.
[19] K.P.W. Dissanayake, W. Wu, N. Hien, T. Sun, K.T.V. Grattan, Graphene-oxide-coated long-period grating-based fiber optic sensor for relative humidity and external refractive index, J. Lightwave Technol. 36 (2018) 1145–1151, https://doi.org/10.1109/jlt.2017.2756097.
[20] S. Liu, H. Meng, S. Deng, Z. Wei, F. Wang, C. Tan, Fiber humidity sensor based on a graphene-coated core-offset Mach–Zehnder interferometer, IEEE Sens. Lett. 2 (2018) 1–4, https://doi.org/10.1109/lsens.2018.2849750.
[21] B. Du, D. Yang, Y. Ruan, P. Jia, H. Ebendorff-Heidepriem, Compact plasmonic fiber tip for sensitive and fast humidity and human breath monitoring, Opt. Lett. 45 (2020) 985–988, https://doi.org/10.1364/OL.381085.
[22] B. Du, D. Yang, X. She, Y. Yuan, D. Mao, Y. Jiang, et al., MoS2-based all-fiber humidity sensor for monitoring human breath with fast response and recovery, Sens. Actuators B Chem. 251 (2017) 180–184, https://doi.org/10.1016/j.snb.2017.04.193.
[23] Y. Zhao, S. Liu, J. Luo, Y. Chen, C. Fu, C. Xiong, et al., Torsion, refractive index, and temperature sensors based on an improved helical long period fiber grating, J. Lightwave Technol. 38 (2020) 2504–2510, https://doi.org/10.1109/jlt.2019.2962898.
[24] C. Fu, B. Yu, Y. Wang, S. Liu, Z. Bai, J. He, et al., Orbital angular momentum mode converter based on helical long period fiber grating inscribed by hydrogen–oxygen flame, J. Lightwave Technol. 36 (2018) 1683–1688, https://doi.org/10.1109/jlt.2017.2787120.
[25] C. Fu, P. Li, Z. Bai, Y. Wang, Helical long period fiber grating inscribed in elliptical core polarization-maintaining fiber, IEEE Access 9 (2021) 59378–59382, https://doi.org/10.1109/access.2021.3073735.
[26] G. Yin, Y. Wang, C. Liao, J. Zhou, X. Zhong, G. Wang, et al., Long period fiber gratings inscribed by periodically tapering a fiber, IEEE Photonics Technol. Lett. 26 (2014) 698–701, https://doi.org/10.1109/lpt.2014.2302901.
[27] L. Zhang, Y. Liu, Y. Zhao, T. Wang, High sensitivity twist sensor based on helical long-period grating written in two-mode fiber, IEEE Photonics Technol. Lett. 28 (2016) 1629–1632, https://doi.org/10.1109/lpt.2016.2555326.
[28] T. Zou, J. Zhong, S. Liu, G. Zhu, Y. Zhao, J. Luo, et al., Helical intermediate-period fiber grating for refractive index measurements with low-sensitive temperature and torsion response, J. Light. Technol. 39 (2021) 6678–6685, https://doi.org/10.1109/jlt.2021.3103550.
[29] S. Xuewen, Z. Lin, I. Bennion, Sensitivity characteristics of long-period fiber gratings, J. Lightwave Technol. 20 (2002) 255–266, https://doi.org/10.1109/50.983240.
[30] M. Luo, Q. Wang, Fabrication and sensing characteristics of arc-induced long-period fiber gratings based on thin-cladding fiber, Alex. Eng. J. 59 (2020) 3681–3686, https://doi.org/10.1016/j.aej.2020.06.022.
[31] M. Wang, L. Jiang, S. Wang, X. Tan, Y. Lu, A robust fiber inline interferometer sensor based on a core-offset attenuator and a microsphere-shaped splicing junction, Opt. Laser Technol. 63 (2014) 76–82, https://doi.org/10.1016/j.optlastec.2014.04.002.
[32] H. Luo, Q. Sun, Z. Xu, D. Liu, L. Zhang, Simultaneous measurement of refractive index and temperature using multimode microfiber-based dual Mach-Zehnder interferometer, Opt. Lett. 39 (2014) 4049–4052, https://doi.org/10.1364/OL.39.004049.
[33] C.R. Liao, H.F. Chen, D.N. Wang, Ultracompact optical fiber sensor for refractive index and high-temperature measurement, J. Lightwave Technol. 32 (2014) 2531–2535, https://doi.org/10.1109/jlt.2014.2328356.
[34] W. Bao, F. Chen, H. Lai, S. Liu, Y. Wang, Wearable breath monitoring based on a flexible fiber-optic humidity sensor, Sens. Actuators B Chem. 349 (2021), https://doi.org/10.1016/j.snb.2021.130794.
[35] A. Melikov, J. Kaczmarczyk, Measurement and prediction of indoor air quality using a breathing thermal manikin, Indoor Air 17 (2007) 50–59, https://doi.org/10.1111/j.1600-0668.2006.00451.x.
[36] B. Xu, J. Huang, L. Ding, H. Zhang, H. Zhang, A sensitive ammonia sensor using long period fiber grating coated with graphene oxide/cellulose acetate, IEEE Sens. J. 21 (2021) 16691–16700, https://doi.org/10.1109/jsen.2021.3081745.
[37] Y. Wang, Y. Liu, F. Zou, C. Jiang, C. Mou, T. Wang, Humidity sensor based on a long-period fiber grating coated with polymer composite film, Sensors 19 (2019), https://doi.org/10.3390/s19102263.
[38] J. Hromadka, N.N. Mohd Hazlan, F.U. Hernandez, R. Correia, A. Norris, S. P. Morgan, et al., Simultaneous in situ temperature and relative humidity monitoring in mechanical ventilators using an array of functionalised optical fibre long period grating sensors, Sens. Actuators B Chem. 286 (2019) 306–314, https://doi.org/10.1016/j.snb.2019.01.124.
[39] J. Hromadka, S. Korposh, M.C. Partridges, S.W. James, F. Davis, D. Crump, et al., Multi-parameter measurements using optical fibre long period gratings for indoor air quality monitoring, Sens. Actuators B-Chem. 244 (2017) 217–225, https://doi.org/10.1016/j.snb.2016.12.050.
[40] A. Theodosiou, R. Min, A.G. Leal-Junior, A. Ioannou, A. Frizera, M.J. Pontes, et al., Long period grating in a multimode cyclic transparent optical polymer fiber inscribed using a femtosecond laser, Opt. Lett. 44 (2019), https://doi.org/10.1364/ol.44.005346.
[41] D. Viegas, J. Goicoechea, J.L. Santos, F.M. Araujo, L.A. Ferreira, F.J. Arregui, et al., Sensitivity improvement of a humidity sensor based on silica nanospheres on a long-period fiber grating, Sensors 9 (2009) 519–527, https://doi.org/10.3390/s90100519.

Shen Liu was born in Henan, China, in 1986. He received the M.S. degree in circuit and system from the Chongqing University of Posts and Telecommunications in 2013, and the Ph.D. degree in optical engineering from Shenzhen University, Shenzhen, China, in 2017. From 2017–2018, he was with Aston University, Birmingham, U.K., as a Postdoctoral

Fellow. Since 2018, he has been with Shenzhen University, as an Assistant Professor. He has authoredor and coauthored 11 patent applications and more than 30 journal and conference papers. His current research interests focus on optical fiber sensors, WGMs resonators, and cavity optomechanics.

Wenqi Yan was born in Jiangxi, China, in 1996. She received a B.E. degree in Applied Physics and Materials, from Wuyi University in 2018 with a major in optoelectronic engineering. Her research interests include the design, preparation, and research of optical resonators and grating fiber sensing applications.

Junlan Zhong was born in Jiangxi, China, in 1990. She received the B.E. degree in Engineering in Biomedical Engineering from Jinggangshan, China, in 2013, the M.S. degree in Engineering in Biomedical Engineering from Shenzhen University, China, in 2016, and the Ph.D. degree in Philosophy in Environment Studies from the University of Tsukuba, Japan, in 2017. Since Oct. 2020, she has been at Shenzhen University, Shenzhen, China, as a postdoctoral. Her current research interests focus on optical fiber sensors, WGMs resonators, and biosensors.

Tao Zou was born in Hunan, China, in 1997. He received the B.E. degree in Opto-Electronics Information Science and Engineering from Guilin University of Electronic Technology, in 2019. His current research interests focus on the design and fabrication of helical fiber grating devices and their applications.

Min Zhou was born in Chongqing, China, in 1993. In 2019, She received the M.S. degree from the School of Optoelectronic Engineering, Chongqing University of Posts and Telecommunications, and then pursued the Ph.D. degree at this University. She is currently studying at Shenzhen University as an exchange student. Her current research interests include fiber gratings, orbital angular momentum, and optical fiber sensors.

Peijing Chen was born in Guangdong, China, in 1997. He received a B.E. degree in Applied Physics and Materials, from Wuyi University in 2020 with a major in optoelectronic engineering. His current research interests focus on the design and fabrication of fiber graphene resonators and their applications.

Hang Xiao was born in Fujian, China, in 1998. He received a B.E. degree in Electronic Science and Technology, from Minjiang University in 2020 with a major in optoelectronic engineering. His current research interests focus on the design, and fabrication of fiber graphene resonators and their applications.

Zhiyong Bai was born in Henan, China, in 1984. He received the B.S. degree in physics from Ningbo University, Ningbo, China, in 2008, the M.S. degree in optics from South China Normal University, Guangzhou, China, in 2011, and the Ph.D. degree in optics from Nankai University, Tianjin, China, in 2014. From 2014–2015, he was at the State Grid Electric Power Research Institute as an R&D Engineer. Since 2015, he has been a Postdoctoral Research Fellow with Guangdong and Hong Kong Joint Research Centre for Optical Fiber Sensors, Shenzhen University, Shenzhen, China. His current research interests include optical fiber gratings, orbital angular momentum, and optical fiber sensors.

Yiping Wang was born in Chongqing, China, in 1971. He received the B.Eng.degree in precision instrument engineering from the Xi'an Institute of Technology, China, in 1995 and the M.S. and Ph.D. degrees in optical engineering from Chongqing University, China, in 2000 and 2003, respectively. From 2003–2005, he was with Shanghai Jiao Tong University, China, as a Postdoctoral Fellow. From 2005–2007, he was with the Hong Kong Polytechnic University, as a Postdoctoral Fellow. From 2007–2009, he was with the Institute of Photonic Technology (IPHT), Jena, Germany, as a Humboldt Research Fellow. From 2009–2011, he was with the Optoelectronics Research Centre (ORC), University of Southampton, U.K., as a Marie Curie Fellow. Since 2012, he has been with Shenzhen University, Shenzhen, China, as a Distinguished Professor. He has authored or coauthored a book, 21 patent applications, and more than 240 journal and conference papers. His current research interests focus on optical fiber sensors, fiber gratings, and photonic crystal fibers. Prof. Wang is a Senior Member of the Optical Society of America and the Chinese Optical Society.